Phased Array Antennas

Floquet Analysis, Synthesis, BFNs, and Active Array Systems

ARUN K. BHATTACHARYYA

WILEY-
INTERSCIENCE

A JOHN WILEY & SONS, INC., PUBLICATION

Phased Array Antennas

Phased Array Antennas

Floquet Analysis, Synthesis, BFNs, and Active Array Systems

ARUN K. BHATTACHARYYA

WILEY-
INTERSCIENCE

A JOHN WILEY & SONS, INC., PUBLICATION

Published simultaneously in Canada

Library of Congress Cataloging-in-Publication Data:

Bhattacharyya, Arun.
Phased array antennas: floquet analysis, synthesis, BFNs, and active array systems /
by Arun K. Bhattacharyya.
p. cm.
"A Wiley-Interscience publication."
Includes bibliographical references and index.
ISBN-13: 978-0-471-72757-6
ISBN-10: 0-471-72757-1
1. Phased array antennas. 2. Electronics—Mathematics. I. Title.

TK6590.A6B45 2005
621.382′4—dc22 2005049360

Printed in the United States of America

10 9 8 7 6 5 4 3 2 1

For my Teachers

Contents

Preface

The purpose of this book is to present in a comprehensive manner the analysis and design of phased array antennas and systems. The book includes recent analytical developments in the phased array arena published in journals and conference proceedings. Efforts have been made to develop the concept in a logical manner starting from fundamental principles. Detailed derivations of theorems and concepts are provided to make the book as self-contained as possible. Several design examples and design guidelines are included in the book. The book should be useful for antenna engineers and researchers, especially those involved in the detailed design of phased arrays. The reader is assumed to have a basic knowledge of engineering mathematics and antenna engineering at a graduate level. The book can be used either as a text in an advanced graduate-level course or as a reference book for array professionals.

The book contains 14 chapters that may be broadly divided into three sections. The first section, which includes Chapters 1–6, is mostly devoted to the development of the Floquet modal-based approach of phased array antennas starting with an introductory chapter. The second section, which includes Chapters 7–10, presents applications of the approach to important phased array structures. The third section, which includes Chapters 11–14, is not directly related to the Floquet modal analysis as such; however, it covers several important aspects of a phased array design. This section includes beam array synthesis, array beam forming networks, active phased array systems, and statistical analysis of phased arrays. Several practice problems are included at the end of each chapter to provide a reader an interactive experience. Information on the solution manual and selective software may be available at **http://hometown.aol.com/painta9/**.

Chapter 1 presents a brief discussion on phased array fundamentals. There are two goals of this chapter. First, it gives a basic overview of phased array characteristics. Second, the limitations of conventional first-order analysis of phased array antennas are spelled out. In this way, the reader can comprehend the limitations of the traditional approach and appreciate the need for a higher order analysis (which is developed in the next few chapters). The chapter begins with the definition of

the element pattern followed by the array pattern and array factor. The maximum-gain theorem of a general array antenna is presented next. Scan characteristics of a pencil beam array is discussed in light of gain, grating lobe, and beam-width considerations. The phase-quantization effects are discussed. Prevalent array synthesis procedures for pencil beam arrays are presented. The scope and limitation of this first-order approach is discussed at the end.

Chapter 2 initiates the development of Floquet modal analysis for array antennas, which is one of the main objectives of the book. Using simple analytic means, we show that Floquet modal expansion evolves from Fourier expansion. The relationship between a Floquet mode and observable antenna parameters, such as radiation direction, is then established. Derivation of Floquet modal functions for an arbitrary array grid structure is presented next. Finally, the coupling of a Floquet mode with a guided mode is considered and interesting consequences are discussed.

In Chapter 3 expressions for normalized Floquet modal functions are deduced. The Floquet modal expansion method is illustrated through an example of an infinite array of electric current sources. Two parameters of an array antenna are defined, namely the Floquet impedance and active element pattern, and their significance is discussed in the context of array performance. A detailed discussion of array blindness is also presented. A scattering matrix formulation for an infinite array of rectangular horn apertures is presented.

Chapter 4 demonstrates that the "results of an infinite array analysis" can be utilized to analyze a finite array with arbitrary excitation. In the first part, important theorems and concepts relevant for the development of finite array analysis are presented. It is well known that the most important factor to consider in a finite array analysis is the mutual coupling. It is demonstrated that the mutual coupling between the elements can be determined using infinite array data obtained through a Floquet modal analysis. Next, the active impedances of the elements and the radiation pattern of a finite array with respect to arbitrary amplitude taper are obtained. The chapter concludes with an alternate approach for finite array analysis. This alternate approach relates infinite array characteristics to finite array characteristics through convolution.

It is often beneficial to divide the entire array into a number of identical groups. Such a group, called a subarray, consists of few elements that are excited by a single feed. In Chapter 5, a systematic procedure is presented to analyze an array of subarrays. Using matrix theory it is shown that a subarray impedance matrix can be constructed from the Floquet impedance of a single element. Important characteristic features of an array of subarrays are presented.

Chapter 6 presents the generalized scattering matrix (GSM) approach to analyze multilayer array structures. The chapter begins with the definition of a GSM followed by the cascading rule of two GSMs. Advantages of the GSM approach over a transmission matrix approach are discussed from a numerical stability standpoint. Using the method of moments and modal matching, the GSMs of several important "building blocks" are deduced. The stationary character of the present approach is then established. Convergence of the solution is discussed in detail. The chapter concludes with a discussion of advantages and disadvantages of the GSM approach.

Chapter 7 applies the GSM approach to analyze probe-fed and slot-fed multilayer patch arrays. The radiation and impedance characteristics of patch arrays are presented. The analysis of an electromagnetically coupled (EMC) patch array and stripline-fed patch array with mode suppressing vias are discussed. Results of finite arrays are presented at the end.

Chapter 8 primarily focuses on horn radiators as array elements. It begins with the linearly flared rectangular horns. It is shown that under certain conditions a horn array structure may support surface and leaky waves. The dips and nulls present in active element patterns are explained via surface and leaky wave coupling. The wide-angle impedance matching aspect of a horn array is discussed. Characteristics of step horns, which may be used for enhanced radiation efficiency, are presented. Design guidelines of "high efficiency horns" are presented at the end.

In Chapter 9, the analyses of three important passive printed array structures are presented. They include frequency-selective surfaces (FSSs), screen polarizers, and printed reflect arrays. In the first part of the chapter, features of a single- and two-layer FSS are presented in terms of return loss, copolar, and cross-polar characteristics. The analysis of a horn antenna loaded with an FSS is considered. In the second part, the analysis of a meander line polarizer screen is presented. The chapter concludes with an analysis of a printed reflect-array antenna for linear and circular polarizations. The gain enhancement method of reflect-array antennas is also discussed.

Chapter 10 presents a method for analyzing complex multilayer array structures that have many useful applications. The analysis is very general to handle layers with different lattice structures, periodicities, and axes orientations. In order to perform the analysis, a mapping relation between the modes associated with a local lattice and the global lattice is established. The mapping relation in conjunction with the GSM cascading rule is utilized to obtain the overall GSM of the structure. The methodology is demonstrated by considering two examples of multilayer structures that have practical applications.

Chapter 11 presents various synthesis methods for shaped beam array antennas. The chapter begins with an analysis of a linear array to study the effects of array size and element size on the array pattern. This is followed by Woodward's beam superposition method for obtaining a shaped beam. Next, different optimization algorithms that are commonly employed for beam shaping are presented. Examples of shaped beams using various optimization schemes are provided.

One of the most important tasks in a phased array design is designing the beam forming network (BFN). Chapter 12 presents comprehensive treatments of the most common types of BFNs. The chapter begins with the simplest type of BFN using passive power divider circuits. The Butler matrix BFN that operates on the principle of the FFT (fast Fourier transform) algorithm is considered. Implementations of Butler BFNs using power dividers and hybrids are shown. The operational principle of a Blass matrix BFN is presented next, followed by the Rotman lens design and analysis. The chapter ends with a discussion of digital beam formers and optical beam formers, including their principles of operations, advantages, and limitations.

In Chapter 13, the basic structures and subsystems of active array antennas are presented. The chapter begins with a generic block diagram of an active array. Typical circuit configurations of each block are considered. Important system parameters are defined and discussed in the context of antenna performance. The intermodulation (IM) products caused by the amplifier nonlinearity are studied. Locations and power levels of IM beams are obtained. To aid the array system analysis, the noise temperature and noise figure of active array components are deduced. A typical example of an array system analysis is presented. Various active array calibration methods are presented at the end.

Chapter 14 presents a statistical analysis of an array antenna with respect to the amplitude and phase uncertainties of the amplifiers and phase shifters. The analysis is developed from the fundamental principles of probability theory. The first part deduces the statistics of the array factor in terms of the amplitude and phase errors. To that end, the statistical parameters of the real and imaginary parts of the array factor are obtained. This is followed by a deduction of the probability density function for the far-field intensity. Also obtained are the simplified closed-form expressions of the probability density functions for the far-field intensity at the beam peak, null, and peak side-lobe locations. Approximate expressions for the 95% confidence boundaries are deduced. Finally, the effect of element failure on the array statistics is introduced. The numerical results with and without element failure are presented. Effects of amplitude and phase uncertainties and element failure on side-lobe levels and null depths are shown.

I express my sincere appreciation to the antenna professionals and friends Owen Fordham, Guy Goyette, Eng Ha, Philip Law, Stephen Kawalko, Gordon Rollins, James Sor, Murat Veysoglu, and Paul Werntz for devoting their personal time to review the chapters. Their expert comments and constructive suggestions were invaluable for improving the text. I express my sincere thanks to Kai Chang for his encouragement and recommendation for publication of the book. Thanks are also due to anonymous reviewers for their suggestions. I am thankful to Rachel Witmer and George Telecki of the editorial department and the production editor Lisa VanHorn for their cooperations during the course of the project. I am grateful to my wife, Arundhuti, and daughters, Atreyi and Agamoni, for their encouragement and moral support in writing the book and for their help in proofreading. I express my profound love and gratitude to my mother, who has been a constant inspiration for me. I am indebted to my teachers for teaching me the fundamentals at various stages of my career. This book is dedicated to them as a token of my appreciation of their love and devotions for teaching.

ARUN K. BHATTACHARYYA

El-Sugendo, California
January 2006

CHAPTER ONE

Phased Array Fundamentals: Pattern Analysis and Synthesis

1.1 INTRODUCTION

In this chapter we present an overview of the basic electromagnetic properties of phased array antennas. We begin with the basics and develop useful concepts for the analysis of phased arrays. Important array terminology is introduced to familiarize the reader with the topic. The element pattern, array pattern, and array factor are introduced, leading to a discussion of how element gain and array gain are tied together. Copolarization and cross-polarization as proposed by Ludwig are presented, and the maximum-gain theorem of an array antenna is deduced. Scan characteristics of a pencil beam array are presented with consideration to gain, grating lobes, and beam deviation due to different types of phase shifters. Prevalent aperture synthesis procedures for sum and difference patterns are presented with theoretical details. Emphasis is placed on the foundation and conceptual development of these methods, and a few words on the scope and limitation of this chapter are included at the end.

1.2 ARRAY FUNDAMENTALS

A phased array antenna consists of an array of identical radiating elements in regular order, as shown in Figure 1.1. In a typical array antenna, all the elements radiate coherently along a desired direction. This is particularly true for a pencil beam array where a linear phase progression between the elements is set to accomplish

Phased Array Antennas. By Arun K. Bhattacharyya

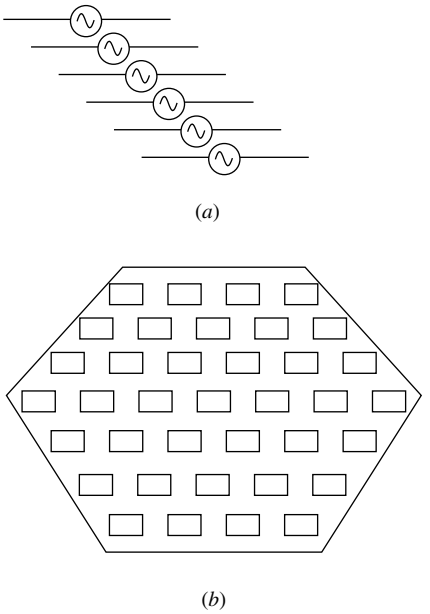

FIGURE 1.1 (*a*) Linear array of dipoles. (*b*) Two-dimensional array of rectangular horns in triangular lattice.

this coherent radiation. For a shaped beam array, however, all the elements do not radiate coherently at a given direction. The shape of the beam decides the amplitude and phase distribution of the array, which is usually nonlinear. In the following sections we will define a few terms that are necessary to understand the radiation of an array antenna.

1.2.1 Element Pattern, Directivity, and Gain

In order to estimate the radiated power of an array antenna in the far-field region, one needs to understand the radiated field intensity of an element in the far-field region. The element pattern is defined as the field intensity distribution of a radiating element as a function of two far-field coordinates, while the radial distance remains constant. In a spherical coordinate system the radiated electric field in the far-field location can be expressed as

$$\vec{E}(r, \theta, \phi) = A\frac{\exp(-jk_0 r)}{r}\vec{e}(\theta, \phi) \tag{1.1}$$

In the above A is a constant which is related to the input excitation of the antenna, $\vec{e}(\theta, \phi)$ is the element pattern, (r, θ, ϕ) is the spherical coordinates of the far-field

point, also known as the observation point, and k_0 is the wave number in free space. It should be pointed out that unless otherwise stated, the radiation pattern is defined at the far-field region where $r >> \lambda_0$, λ_0 being the wavelength in free space. In (1.1) $\vec{e}(\theta, \phi)$ is a complex vector function having components along $\hat{\theta}$- and $\hat{\phi}$-directions only. The radial component does not exist in the far-field region.

The complex directive pattern of an element is the far-field intensity pattern normalized with respect to the square root of the average radiated power per unit solid angle. The total radiated power is determined by integrating the Poynting vector on a spherical surface covering the antenna element as

$$P_r = \iint_{\Omega} \frac{|\vec{E}|^2}{\eta} r^2 d\Omega = \frac{|A|^2}{\eta} \int_0^{2\pi} \int_0^{\pi} |\vec{e}(\theta, \phi)|^2 \sin\theta \, d\theta \, d\phi \tag{1.2}$$

In (1.2) η represents free-space impedance, which is equal to 120π (or 377) ohms. The average power per unit solid angle is

$$P_r^{\text{av}} = \frac{P_r}{4\pi} \tag{1.3}$$

Thus the complex directive pattern of the element becomes

$$\vec{D}(\theta, \phi) = \sqrt{\frac{1}{\eta}} \sqrt{\frac{4\pi}{P_r}} A \, \vec{e}(\theta, \phi) \tag{1.4}$$

Observe that in order to make $\vec{D}(\theta, \phi)$dimensionless the factor $\sqrt{1/\eta}$ is introduced in (1.4). Substituting the expression of P_r from (1.2) in (1.4), we obtain

$$\vec{D}(\theta, \phi) = \frac{\sqrt{4\pi} \, \vec{e}(\theta, \phi)}{\sqrt{\int_0^{2\pi} \int_0^{\pi} |\vec{e}(\theta, \phi)|^2 \sin\theta \, d\theta \, d\phi}} \tag{1.5}$$

In deducing (1.5) we assume $|A| = A$, which we justify by accommodating the complex exponent part of A into the element pattern $\vec{e}(\theta, \phi)$.

The directivity of an element signifies the relative power flux per solid angle with respect to that of an isotropic radiator that radiates an equal amount of power. The directivity at (θ, ϕ) is the square of the magnitude of $\vec{D}(\theta, \phi)$. Usually the directivity is expressed in dBi, where i stands for isotropic. The complex gain pattern of an element is the far-field intensity pattern normalized with respect to

the incident power at the antenna input instead of the total radiated power. Thus the complex gain pattern with respect to the field intensity can be expressed as

$$\vec{G}(\theta, \phi) = A\sqrt{\frac{4\pi}{\eta P_{\text{inc}}}}\,\vec{e}(\theta, \phi) \tag{1.6}$$

In (1.6) P_{inc} is the incident power and A is related to P_{inc}. The gain at a far-field point is given by $|\vec{G}(\theta, \phi)|^2$ [however, at places we use the word "gain" to indicate either $\vec{G}(\theta, \phi)$ or $|\vec{G}(\theta, \phi)|^2$, which can be understood from the context]. Since the total radiated power is reduced by the antenna mismatch loss and other radio-frequency (RF) losses, the gain does not exceed the directivity.

1.2.2 Copolarization and Cross-Polarization

As mentioned before, the radiated field emanating from a radiating source has two mutually orthogonal components along $\hat{\theta}$ and $\hat{\phi}$, respectively. For linearly polarized radiation, the copolarization vector essentially is the preferred electric field vector. The cross-polarization vector is orthogonal to both the copolarization vector and the direction of radiation. One can define the preferred polarization direction according to one's preference. However, we will follow *Ludwig's third definition* [1] as it is well accepted by the antenna community and has practical significance. According to this definition, the copolarization and cross-polarization components at a far-field point (θ, ϕ) of an electric current source (or electric field source for an aperture antenna) polarized along the x-direction are defined as

$$e_{\text{co}}(\theta, \phi) = \vec{e}(\theta, \phi) \cdot [\hat{\theta}\cos\phi - \hat{\phi}\sin\phi] \tag{1.7a}$$

$$e_{\text{cr}}(\theta, \phi) = \vec{e}(\theta, \phi) \cdot [\hat{\theta}\sin\phi + \hat{\phi}\cos\phi] \tag{1.7b}$$

where $\vec{e}(\theta, \phi)$ represents the far electric field pattern of the source. The above definition is consistent with the standard pattern measurement method where aperture of the antenna under test (AUT) is placed on the $z = 0$ plane and the probe antenna is mounted on a rigid rod such that the probe always remains perpendicular to the rod. The probe end of the rod is free to move along the great circles on ϕ-constant planes (Figure 1.2) without any twist, while the other end is fixed at a reference point on the AUT. For the copolarization measurement, the probe must be aligned with the principal polarization direction when it is situated at the bore sight ($\theta = 0$) of the AUT. Under these conditions, the orientation of the probe for an arbitrary probe location defines the copolarization vector. The cross-polarization vector is perpendicular to the copolarization vector and the radius vector.

The copolarization gain is of practical importance because it is used for estimating the amount of power received by a receiving antenna, which is polarized at the same sense of the transmitting antenna. The copolarization gain can be calculated by taking the copolarization component of $\vec{e}(\theta, \phi)$ in (1.6). The cross-polarization gain

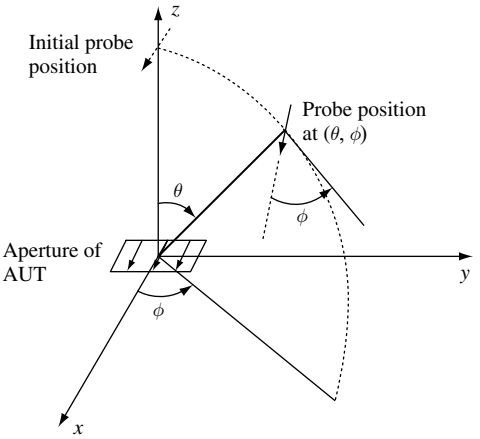

FIGURE 1.2 Antenna copolar pattern measurement scheme following Ludwig's third definition. Notice that the probe maintains an angle ϕ with the tangent of the circle (θ-direction) shown by the dotted line, which is consistent with (1.7a). The principal polarization of the AUT is along x.

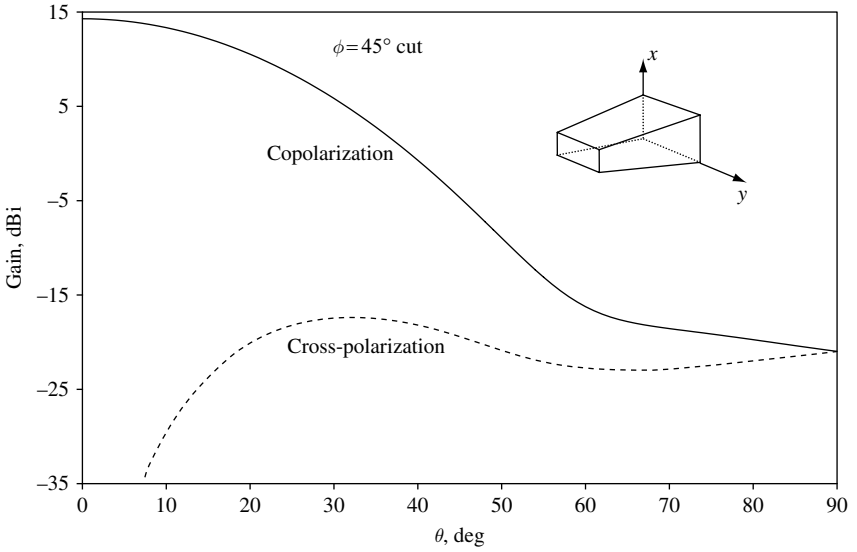

FIGURE 1.3 Copolarization and cross-polarization patterns of a square horn of length $3\lambda_0$ and of aperture size $1.6\lambda_0 \times 1.6\lambda_0$. The input waveguide dimension is $0.6\lambda_0 \times 0.3\lambda_0$ and is excited by the TE_{01} mode.

can be obtained similarly. Figure 1.3 shows the copolarization and cross-polarization gain patterns of a linearly flared horn. The cross-polarization field intensity vanishes along the two principal plane cuts (E- and H-plane cuts); therefore we choose the diagonal plane cut for the plot.

It is worth mentioning that there is no preferred direction for a circularly polarized radiation. The right and left circular polarization unit vectors (rcp and lcp) for $\exp(j\omega t)$ time dependence are defined as

$$\hat{e}_{\text{rcp}}(\theta, \phi) = \frac{1}{\sqrt{2}}[\hat{\theta} - j\hat{\phi}] \tag{1.8a}$$

$$\hat{e}_{\text{lcp}}(\theta, \phi) = \frac{1}{\sqrt{2}}[\hat{\theta} + j\hat{\phi}] \tag{1.8b}$$

Notice, the polarization vectors are mutually orthogonal because $\hat{e}_{\text{rcp}} \cdot \hat{e}^*_{\text{lcp}} = 0$.

1.2.3 Array Pattern

The radiated field of an array essentially is the summation of the individual element fields. It can be shown that the far-field pattern of an array of identical elements can be represented by a product of two quantities, namely the *element pattern* and the *array factor*. The element pattern signifies the radiation behavior of an individual element and the array factor signifies the arraying effect, including array architecture and relative excitations of the elements. To establish this relation we consider a linear array of N identical elements along the x-axis with element spacing a as shown in Figure 1.4. The excitation coefficient $A_n (n = 1, 2, ..., N)$ is assumed to be a complex number incorporating amplitude and phase in a single entity. Invoking (1.1) and applying superposition of the individual fields, the array field can be expressed as

$$\begin{aligned}\vec{E}_{\text{array}} = A_1 \frac{\exp(-jk_0 r_1)}{r_1}\vec{e}(\theta, \phi) + A_2 \frac{\exp(-jk_0 r_2)}{r_2}\vec{e}(\theta, \phi) + \cdots \\ + A_N \frac{\exp(-jk_0 r_N)}{r_N}\vec{e}(\theta, \phi)\end{aligned} \tag{1.9}$$

In (1.9) $r_n (n = 1, 2, ..., N)$ is the distance from the nth element to the observation point located at the far field. For $r_n >> Na$ we can have the following approximation:

$$r_n \approx r_1 - (n-1)a \sin\theta \cos\phi \qquad n = 1, 2, \ldots, N \tag{1.10}$$

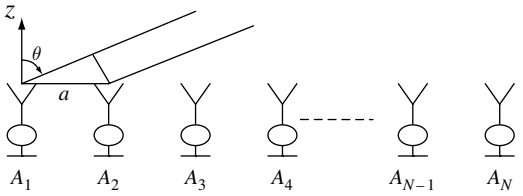

FIGURE 1.4 Linear array of N elements. The elements are situated along the x-axis.

The above approximation should be used for the r_n that lies inside the argument of the complex exponential function, because complex exponential functions are highly oscillatory. For the r_n in the denominator, however, a more crude approximation, namely $r_n \approx r_1$, is admissible because $1/r$ is a slow-varying function for large r. Thus (1.9) becomes

$$\vec{E}_{\text{array}} = \vec{e}(\theta, \phi)\frac{\exp(-jk_0 r_1)}{r_1}[A_1 + A_2 \exp(jk_0 a \sin\theta\cos\phi) + \cdots + A_N \exp\{jk_0(N-1)a\sin\theta\cos\phi\}] \tag{1.11}$$

The quantity inside the square bracket is known as the array factor (AF) for a linear array. Ignoring the radial dependence part we observe that the array pattern reduces to a product of the element pattern and the array factor. For a two-dimensional array a similar development results in the following array factor:

$$\text{AF}(\theta, \phi) = \sum_{n=1}^{N} A_n \exp[jk_x x_n + jk_y y_n] \tag{1.12}$$

In (1.12), (x_n, y_n) represents the coordinate of the nth element and k_x, k_y are

$$k_x = k_0 \sin\theta\cos\phi \qquad k_y = k_0 \sin\theta\sin\phi \tag{1.13}$$

Figure 1.5 depicts a typical pattern of a linear array. For this plot 20 elements that are uniformly exited and spaced at $1\lambda_0$ apart are used. The plot shows the relative

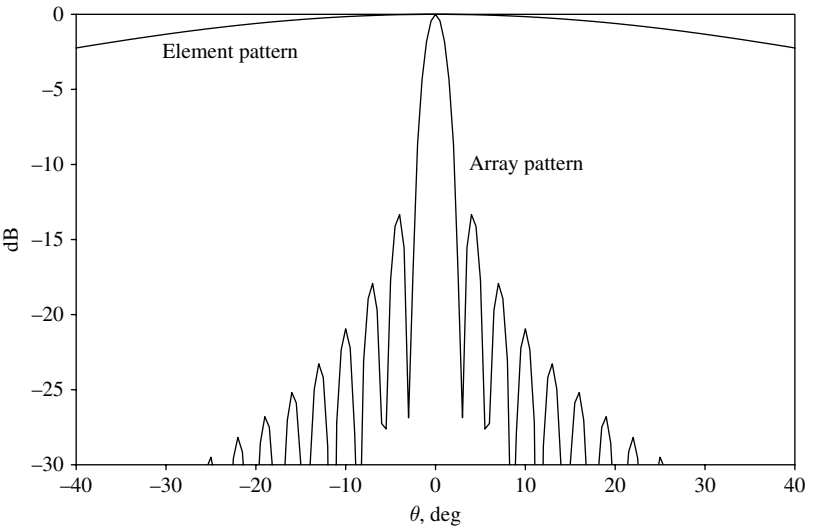

FIGURE 1.5 Radiation pattern of a uniformly excited linear array with 20 elements. Element spacing λ_0.

field intensity (with respect to the peak field intensity) versus θ on $\phi = 0°$ plane. To examine the arraying effect, the element pattern is also plotted. Evidently, the array beam width is much smaller than the element beam width, implying a high level of beam focusing capability of the array.

The array pattern deduced in (1.11) assumes identical element patterns for all the elements. This is not rigorously valid because even if the elements have identical shapes they have different surroundings.[1] For instance, the edge element of an array will have a different radiation pattern than that of the center element. However, in most applications the *identical radiation pattern* assumption may be reasonable, particularly in the bore-sight region where small variations in the element patterns do not introduce an error beyond the acceptable limit.

1.2.4 Array Gain

The gain of an array can be determined after normalizing the field intensity in (1.11) with respect to the total incident power of the array. It is convenient to use the element gain pattern as the element pattern in (1.11) because the field intensity is already normalized with respect to its incident power. The array pattern thus can be written as

$$\vec{E}_{\text{array}} = \vec{G}(\theta, \phi)[A_1 + A_2 \exp(jk_0 a \sin\theta \cos\phi) + \cdots + A_N \exp\{jk_0(N-1)a \sin\theta \cos\phi\}] \tag{1.14}$$

In (1.14) the element gain pattern, $\vec{G}(\theta, \phi)$, is normalized so that

$$\int_0^{2\pi} \int_0^{\pi} |\vec{G}(\theta, \phi)|^2 \sin\theta \, d\theta \, d\phi = 4\pi(1 - L) \tag{1.15}$$

where L is the antenna loss factor. We must emphasize here that for the array gain determination we consider A_n as the normalized incident voltage or current [not to be confused with the A in (1.6)] for the nth element such that $|A_n|^2$ becomes its incident power. Thus the total incident power of the array is given by

$$P_{\text{inc}} = \sum_{n=1}^{N} |A_n|^2 \tag{1.16}$$

Thus the complex gain pattern of the array can be written as

$$\vec{G}_{\text{array}}(\theta, \phi) = \vec{G}(\theta, \phi) \frac{\sum_{n=1}^{N} A_n \exp(jk_0 na \sin\theta \cos\phi)}{\sqrt{\sum_{n=1}^{N} |A_n|^2}} \tag{1.17}$$

[1] The radiation pattern of an element, including the effects of surrounding elements, is known as the *active element pattern*. Analysis of the active element pattern will be considered in a later chapter.

The co- and cross-polarization gain patterns simply are the corresponding components of $\vec{G}_{\text{array}}(\theta, \phi)$.

The above array gain pattern expression is rigorously valid if the following two conditions are satisfied: (a) The element gain pattern $\vec{G}(\theta, \phi)$ is measured or computed in array environment with all other elements match terminated, that is $\vec{G}(\theta, \phi)$ represents active element gain pattern, and (b) elements have identical active element patterns. In reality condition (b) is not generally satisfied because the active element pattern differs from element to element. For such situations (1.17) can be modified as

$$\vec{G}_{\text{array}}(\theta, \phi) = \frac{\sum_{n=1}^{N} A_n \vec{G}_n(\theta, \phi) \exp(jk_0 na \sin\theta \cos\phi)}{\sqrt{\sum_{n=1}^{N} |A_n|^2}} \tag{1.18}$$

In (1.18) $\vec{G}_n(\theta, \phi)$ represents the active element gain pattern for the nth element of the array. Figure 1.6 is a pictorial definition of the active element pattern.

1.2.5 Maximum-Array-Gain Theorem

The maximum-gain theorem yields the optimum excitation condition of the array to achieve maximum gain along a desired direction. The statement and the proof of the theorem follow.

Statement The maximum gain (magnitude) of an array at a desired direction occurs if the incident voltage (or current) is proportional to the complex conjugate of the active element gain along the desired direction.

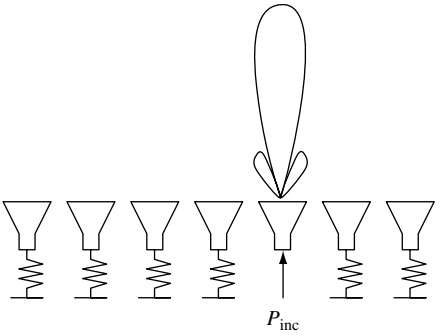

FIGURE 1.6 Pictorial definition of the active element pattern of an element in a seven-element array. The element under consideration is excited while the other elements are match terminated.

Proof In order to prove the above theorem we consider (1.18). Without loss of generality we can assume that the total incident power is unity, implying

$$\sum_{n=1}^{N} |A_n|^2 = 1 \tag{1.19}$$

Then the array gain pattern becomes

$$\vec{G}_{\text{array}}(\theta, \phi) = \sum_{n=1}^{N} A_n \vec{G}_n(\theta, \phi) \exp(jk_0 na \sin\theta \cos\phi) \tag{1.20}$$

We will consider the copolar gain at (θ, ϕ); therefore we extract the copolar component in both sides of (1.20), leaving

$$G^{\text{co}}_{\text{array}}(\theta, \phi) = \sum_{n=1}^{N} A_n G^{\text{co}}_n(\theta, \phi) \exp(jk_0 na \sin\theta \cos\phi) \tag{1.21}$$

From triangular inequality [2] we know that the magnitude of the sum of complex numbers is less than or equal to the sum of their magnitudes. Applying this in (1.21) we write

$$\begin{aligned} |G^{\text{co}}_{\text{array}}(\theta, \phi)| &= |\sum_{n=1}^{N} A_n G^{\text{co}}_n(\theta, \phi) \exp(jk_0 na \sin\theta \cos\phi)| \\ &\leq \sum_{n=1}^{N} |A_n G^{\text{co}}_n(\theta, \phi) \exp(jk_0 na \sin\theta \cos\phi)| = \sum_{n=1}^{N} |A_n||G^{\text{co}}_n(\theta, \phi)| \end{aligned} \tag{1.22}$$

The equality holds if

$$A_n G^{\text{co}}_n(\theta, \phi) \exp(jk_0 na \sin\theta \cos\phi) = |A_n| \cdot |G^{\text{co}}_n(\theta, \phi)| \tag{1.23}$$

for all n. To satisfy (1.23), the phase of A_n must be negative of the phase of $G^{\text{co}}_n(\theta, \phi) \exp(jk_0 na \sin\theta \cos\phi)$. Symbolically,

$$\angle A_n = -\angle G^{\text{co}}_n - k_0 na \sin\theta \cos\phi \tag{1.24}$$

If (1.24) is satisfied, then the magnitude of the copolar gain of the array along the (θ, ϕ) direction becomes

$$|G^{\text{co}}_{\text{array}}(\theta, \phi)| = \sum_{n=1}^{N} |A_n| \cdot |G^{\text{co}}_n(\theta, \phi)| \tag{1.25}$$

Equation (1.24) yields the phase of the excitations; however, the magnitude of A_n for maximum gain is yet to be found. Toward that effort we maximize (1.25) subject